Clinical Spectroscopy 3 (2021) 100015

Contents lists available at ScienceDirect

Clinical Spectroscopy

journal homepage: www.sciencedirect.com/journal/clinical-spectroscopy

Could Raman spectroscopy distinguish between *P. falciparum* and *P. vivax* Infection?

Malwina Birczyńska-Zych [a,b], Jacek Czepiel [a,b], Maria Łabanowska [c], Martyna Kraińska [c], Grażyna Biesiada [a,b], Paulina Moskal [c], Mateusz Kozicki [c,1], Aleksander Garlicki [a,b], Aleksandra Wesełucha-Birczyńska [c,*]

[a] Department of Infectious and Tropical Diseases, Jagiellonian University, Medical College, Jakubowskiego 2, 30-688 Kraków, Poland
[b] University Hospital in Kraków, Jakubowskiego 2, 30-688 Kraków, Poland
[c] Faculty of Chemistry, Jagiellonian University, Gronostajowa 2, 30-387 Kraków, Poland

ARTICLE INFO

Keywords:
Malaria
Plasmodium falciparum (*P. falciparum*)
Plasmodium vivax (*P. vivax*)
Principal Component Analysis (PCA)
Raman microspectroscopy

ABSTRACT

The erythrocytes obtained from patients diagnosed with *Plasmodium falciparum* or *Plasmodium vivax* infection (two groups of five patients each) and treated in the Department of Infectious Diseases, University Hospital in Kraków, were measured using the Raman spectroscopy method (1–2 cells of each patient) and then compared with the results from these patients during their convalescence. Principal Component Analysis (PCA) was used to determine the variance between the Raman spectra. Changes in the heme structure were observed by the ν_4 oxidation state marker and by other heme and hemozoin marker bands, as well as protein side chains marker bands. The recognized Raman bands allow to differentiate changes taking place in the red blood cells during the development of *Plasmodium falciparum* from *Plasmodium vivax*. The 1385 cm^{-1} Asp band along with the 1587 cm^{-1} Gln vibrations at the beginning of hospitalization specify the invasion of *P. falciparum* that occurs with the basigin receptor which requires respective protein glycosylation. The 1361 cm^{-1} and 1544 cm^{-1} Trp bands indicate the invasion stage of the *P. vivax* parasite, and the formation of the ligand-receptor complex. To our knowledge, this is the first Raman spectroscopic observation that we can distinguish *Plasmodium species*.

1. Introduction

Malaria is still one of the most deadly infectious diseases, that affects more than 500 million people annually, causing between 1 and 3 million deaths. According to the World-malaria-report-2019 most malaria cases in 2018 were in the African Region (93%), then in the South-East Asia Region 3.4% cases, and next in the Eastern Mediterranean Region with 2.1% [1]. Children aged under 5 years are the group affected by malaria with the most risk. In 2017, the 61% of all malaria deaths worldwide were reported in this group.

In Poland malaria was endemic up to the middle of 60th years of the 20th century [2]. Since then, malaria transmission has not been observed. Nowadays people that are infected with malaria are usually travelers, workers coming back home for holidays, students returning from international exchanges, soldiers serving on peace-keeping missions and missionaries [3,4]. In the last report of the National Institute of Public Health, Poland, in 2019 there were 24 cases of malaria reported, in 2018 there were 28 cases. Fortunately no fatal cases were noticed [3].

Malaria is an infectious disease caused by *Plasmodium* parasites. Humans are the intermediate host for *Plasmodium*, infected female *Anopheles* mosquitoes are malaria vectors. There are five parasite species that cause malaria in humans, and two of these species – *P. falciparum* and *P. vivax* – cause the greatest threat. It is known that *P. falciparum* is the most dangerous malaria agent, while *P. vivax* is a cause of mostly non-severe malaria [5–7]. This assessment is due, inter alia, to the fact that the actual data on *P. vivax* mortality are still uncertain [8–10].

The first symptoms of infection – fever, headache, and chills – may be mild and difficult to recognize as malaria. The technique which remains as a "gold standard" in diagnostics is an examination under the microscope a drop of the patient's blood, spread out as a blood smear on a microscope slide [11,12]. Prior to examination, the specimen is stained (with the Giemsa method) to give the parasites a distinctive appearance.

* Corresponding author.
E-mail address: birczyns@chemia.uj.edu.pl (A. Wesełucha-Birczyńska).
[1] Current Mateusz Kozicki afiliation: Building Research Institute, Filtrowa 1, Warszawa, Poland.

https://doi.org/10.1016/j.clispe.2021.100015
Received 30 December 2020; Received in revised form 15 September 2021; Accepted 25 September 2021
Available online 29 September 2021
2666-0547/© 2021 The Author(s). Published by Elsevier B.V. This is an open access article under the CC BY-NC-ND license (http://creativecommons.org/licenses/by-nc-nd/4.0/).

This method allows the malaria diagnosis, as well as monitoring the treatment. Early diagnosis and treatment of malaria reduces disease progression and mortality [13,14]. It also contributes to reduce malaria transmission. The distinction between the *Plasmodium* is important for treatment selection and patient's prognosis [15,16]. Therefore, many efforts are taken to find a proper and quick diagnostic method of malaria. For example, research is being conducted into the diagnostic application of spectroscopic methods [17].

P. falciparum and *P. vivax* exhibit some different features of the life cycle. It may be a reason of other specificity of changes in erythrocytes due to parasite heterogeneity [18–22]. Feature allowing to differentiate these two malaria species is the fact that *Plasmodium vivax* forms hypnozoite forms in humans liver [23] and that their erythrocyte cycle occurs mainly in reticulocytes [24]. Another difference in the life cycle of *P. vivax* compared to *P. falciparum* is the rate of gametocyte development. In the case of *P. vivax*, this process occurred rapidly [25].

Raman spectroscopy traces successfully heme modification during the asexual erythrocyte cycle. The merozoite invades the host's red blood cell, creating a food vacuole separated from the host cell's cytoplasm [26]. Degradation of hemoglobin begins already in the ring-phase, but the vast majority of degradation occurs in the 6–12 h stage of trophozoite. The heme concentration in the food vacuole quickly becomes remarkably high, and the consequence of the elevated heme concentration oxidative stress is increased [26,27]. Trophozoites contain an activity that catalyzes the formation of hemozoin and this process also detoxifies the heme (which is toxic for *Plasmodium*) [28].

Apart from the changes taking place in the heme structures of the infected erythrocyte by *Plasmodium* also other changes were successfully observed by Raman spectroscopy. It introduces disorder in the phospholipids of erythrocytes membrane. *Trans* configuration, characteristic for healthy red blood cells, transforms and the number of *gauche* conformers increases, therefore the membrane molecular arrangement leads to changes in the structure and fluidity [4,29–31]. The C-C backbone and C-H stretching vibrations of the *trans* and *gauche* conformations differ and the corresponding marker bands appear at different wavenumber positions in the Raman spectra [29,31–33]. *Plasmodium* invasion proceeds through a series of complex stages of receptor-ligand interaction [6,34]. This activity of the parasite triggers the movement of numerous proteins through a series of membranes inside the cell and through the cytoplasm. *Plasmodium spp*. introduced theirs own proteins into erythrocyte plasma membrane in the first seconds of the invasion of the erythrocytes, in the phase of strong binding and finally in internalization [21]. *P. falciparum* Erythrocyte Membrane Protein 1 (PfEMP1) is the major virulence factor on the surface of *P. falciparum*-infected RBCs [35,36]. A biological analysis has shown that the majority glycoproteins are associated with virulence factors of medically significant pathogens [37]. The membrane protein which is characteristic for *P. vivax* invasion is Transferrin receptor (TfR) [38]. This protein is rich in Tryptophane [39,40].

In the present study, we have examined the erythrocytes obtained from patients diagnosed with *P. falciparum* or *P. vivax* infection at the Department of Infectious and Tropical Diseases, University Hospital in Kraków, and then compared it with the medical results obtained from these patients during their convalescence. The aim of this work was both- to study RBC across the patients recovery as well as comparing *P. falciparum* vs *P. vivax* effect on erythrocyte. This work seems to be unique due to Raman measurements performed on samples taken from patients blood. It is especially valuable for *P. vivax* as there is limited posibility to culture *P. vivax in vitro* [41,42]. Although the *Plasmodium* affect similar on RBCs [43,44], but we expect that the recognized Raman bands will allow us to distinguish changes in red blood cells during the development of *P. falciparum*, in relation to *P. vivax*. To our knowledge, this is the first observation in which we can distinguish *Plasmodium* spp. by analyzing their activity through their influence on the erythrocytes of hospitalized patients using Raman spectroscopy. This could contribute to a different and perhaps faster diagnostics carried out in parallel with traditional methods.

2. Materials and methods

2.1. Patients and medical standard diagnostic tests

The patients who took part in our research were cases with imported malaria from African and Asian endemic regions: two African students studying in Poland, three tourists, two people working in endemic areas, two medical mission volunteers and one missionary, see Fig. 1. They were hospitalized at the University Hospital the Department of Infectious Diseases in Kraków. Two types of malaria were diagnosed - caused by *P. falciparum* and *P. vivax*, two groups of five patients each were studied using Raman microspectroscopy method. Standard medical procedures, tests and treatment, were performed according to the generally accepted methods. The suspicion of malaria was made based on the patient's travel history, symptoms, and the physical findings at examination, laboratory tests, and malaria rapid diagnostic tests (OptiMAL-IT Rapid Malaria Test Kit, Bio-Rad, France). For a definitive diagnosis the malaria parasites were identified by microscopic examination. In whole research group there were 21 patients, 15 diagnosed with *P. falciparum* and 6 with *P. vivax*. The most severe course was analysed in 5 patients in each group.

These studies were conducted in accordance with the guidelines for good clinical practice (GCP) and according to Ethical Principles for Medical Research Involving Human Subjects (Declaration of Helsinki). The study was approved by the local Bioethics Committee.

2.2. Blood samples for Raman measurements

The blood from patients with malaria was obtained by venipuncture at the beginning of hospitalization, and also from these patients as they were recovering, at the end of hospitalization. The blood was placed in tubes containing heparin as an anti-coagulant and was transported to the Raman laboratory without delay. Then it was deposited as a blood film so that it could be measured. The cells were allowed to settle for about ten minutes prior to measurement.

2.3. Raman microspectroscopy

A Renishaw inVia spectrometer, working in a confocal mode, connected to a Leica microscope, was used for the measurement of a single cell Raman spectrum. The beam from a 514.5 nm Ar^+ ion Modu Laser was focused by a 100 × magnifying, high numerical aperture (NA = 0.9) top class Leica objective for standard applications. Raman light was dispersed by a diffraction grating with 2400 grooves per mm. The laser power was kept low, ca. 1–3 mW at the sample, to ensure the minimum invasion to the cells. Pre-processing of Raman spectra, smoothing and a baseline correction, was performed with the Renishaw WiRE 3.4 and 2.0 software.

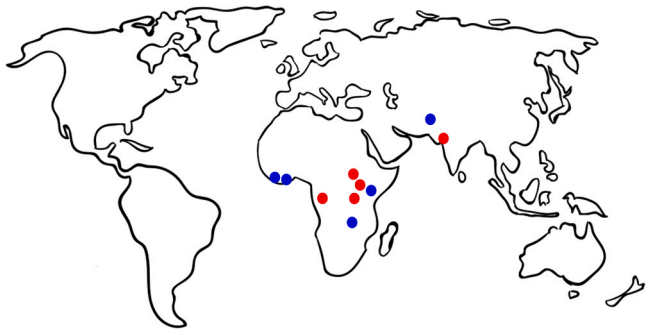

Fig. 1. Map showing malaria cases analyzed in the work, *P. falciparum* (red dots), *P. vivax* (blue dots).

2.4. Statistical analysis of the results of medical standard diagnostic tests

The results of the blood morphology for the entire research group and also for severe cases were statistically analyzed by calculating the arithmetic mean of the results and the standard population deviation function in Excel software. These data, presented in the form of graphs, are included in the Supplementary materials, Figs. S1–S3.

2.5. Principal component analysis

Principal Component Analysis (PCA) allows for the determination of the variance between the Raman spectra of a single RBCs of patients, with identified *P. falciparum* or *P. vivax* infection, obtained at the beginning of hospitalization (90 and 78 spectra, respectively), and also as patients were recovering, at the end of hospitalization (119 and 112 spectra, respectively). Investigation of the collected spectra were made within one *Plasmodium species* evaluating the beginning and the end of hospitalization. Additionally there were performed analyses comparing the modifications of the red blood cells by the two *Plasmodium species* . A PCA was performed and discussed in the four spectral regions using Unscrambler X software packages (v. 10.3, CAMO Software, Oslo, Norway). The Raman spectra were pre-processed: smoothed using a Savitzky–Golay smoothing algorithm (thirteen smoothing points), baseline corrected and unit vector normalized.

3. Results and discussion

3.1. Malaria and the results of the selected medical tests

As it was mentioned before for malaria definitive diagnosis, treatment planning and monitoring, the microscope identification of blood smear with Giemsa staining should be performed. The results of % parasitemia for all patients who participated in the study is presented in Fig. 2. In Fig. 2A there is showed the mean parasitemia for all patients with *P. falciparum* and with *P. vivax*, the red and blue line, respectively. In Fig. 2B there is the parasitemia obtained from the patients with the most severe course of the disease. It can be observed that for patients infected by *P. falciparum* there is a much higher parasitemia level, especially in the case of the patient with the most severe course of the disease (Fig. 2B).

Other selected laboratory results of the malaria patients are presented and commented in Supplementary material.

3.2. The appearance of the invaded red blood cells

Structural changes, resulting from the invasion of red blood cells by malaria parasites, are also associated with alteration in the appearance of infected erythrocytes, see Fig. 3.

The cells into which the parasite has invaded, compared to normal erythrocytes, are more rigid, less deformable and they appear more rounded and convex [45]. These features can lead to their complete immobilization in the microcirculation and in conjunction with adhesion appear to be a critical process for the maintenance of parasite virulence [29]. The stiffening of the RBC cell skeleton was observed as an effect of the action of other toxins as well [46]. It is believed that cytoadherence may have evolved to minimize the exposure of rigid parasitic cells in the spleen, thus minimizing spleen sequestration and destruction [45]. It is the subject of research whether modifications of the mechanical properties of erythrocytes are related to the growth of the parasite and the export of its proteins through the membrane or are they essential for the development of the parasite [47].

3.3. Raman microspectroscopy results

Raman spectra obtained from data averaged on a first and tenth day of hospitalization for the representative patients diagnosed with

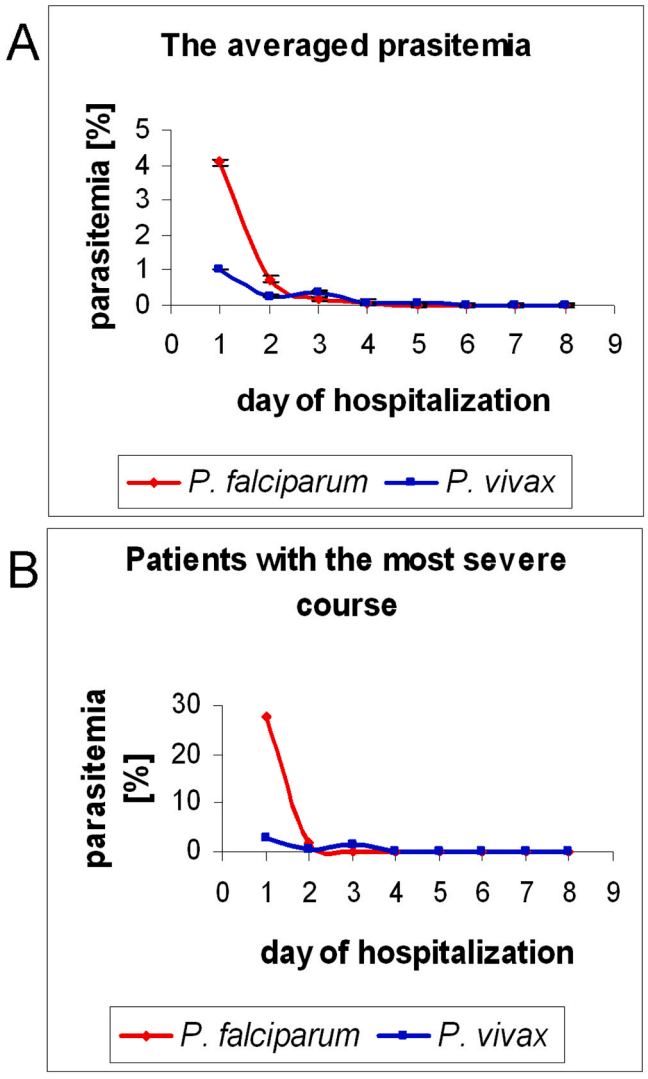

Fig. 2. The parasitemia during the course of the treatment of the malaria infected patients. The red line shows the levels for the patients diagnosed with *Plasmodium falciparum*, the blue one- *Plasmodium vivax*; (A) average results for all patients (B) data from the patients with the most severe course of the disease.

P. falciparum and *P. vivax* are presented in Fig. 4. Spectra for *Plasmodium* infected red blood cells are similar, it is difficult to identify the characteristics associated with a particular species of parasite. The leading difference is related to the structure of oxy- and deoxy- hemoglobin vibrations, resulting from the activity of the *Plasmodium* and consequently leading to changes in the red blood cells. Band assignments were carried out by recognizing and characterizing the vibrations of metalloporphyrins that model heme vibrations, see Table S1 [48–53]. However, the specificity of resonance excitation on the 514.5 nm line, close to Q_{0-0} band, is a decrease in relative intensity of the ν_2, ν_3 and ν_4 symmetric modes, so the intensity enhancement may not seem so significant [54]. Although the blood was collected and measured on the 1st day of patient hospitalization, the various stages of malaria parasite development cannot be excluded. On the last 10th day of hospitalization of the treated patients, the effects of parasite activity should disappear, which determines a parasitemia level equal to zero.

The representative spectra from the first and the last day of hospitalization, for both of the studied types of parasitic protozoa of the genus *Plasmodium* were compared in Fig. 4. The PCA model was built on the basis of RBCs Raman spectra of patients infected with *P. falciparum* and *P. vivax*, at the beginning and at the end of hospitalization, which gave

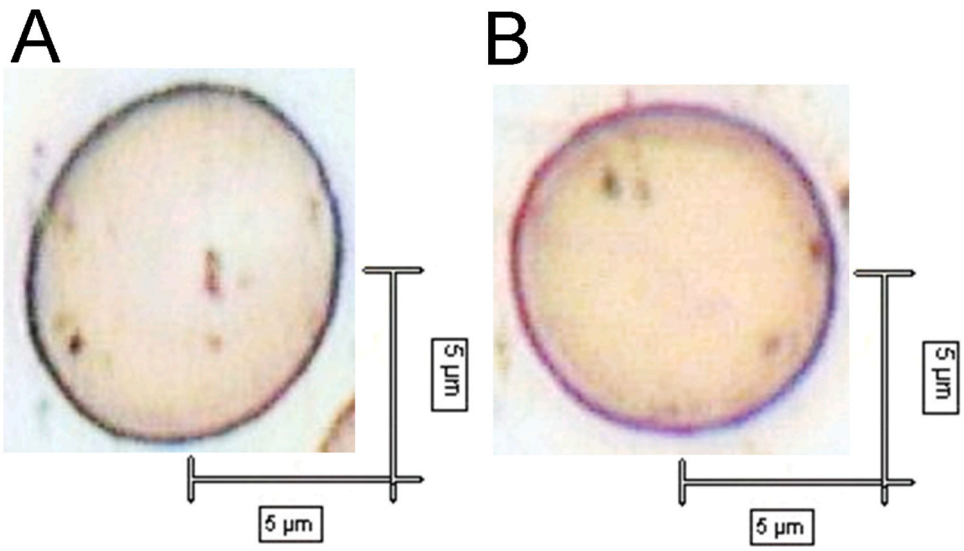

Fig. 3. Microphotographs of infected RBC with (A) *P. falciparum*, (B) *P. vivax*, the first day of hospitalization.

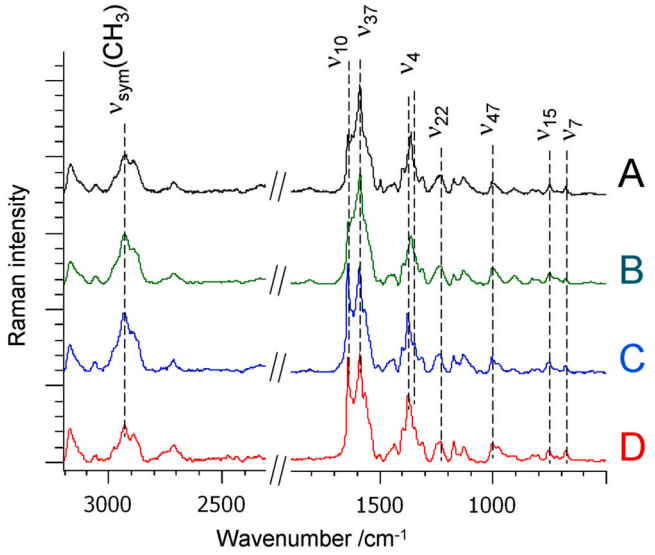

Fig. 4. Raman spectra showing the most prominent peaks in the ranges of 1900–1000 cm^{-1} and 3200–2300 cm^{-1} of RBCs patients infected with, (A) *P. falciparum*, (B) *P. vivax*, the 1st day of hospitalization, and (C) *P. falciparum*, (D) *P. vivax*, the 10st day of hospitalization, excitation laser line at 514.5 nm; 100 × magnification objective (NA= 0.90) [29,31,48–55,59].

four correlations, *Pf*1 (*P. falciparum* the 1st day of hospitalization) vs *Pf*10 (*P. falciparum* the 10th day of hospitalization), *Pv*1 (*P. vivax* the 1st day of hospitalization) vs *Pv*10 *Pv*1 (*P. vivax* the 10th day of hospitalization), *Pf*1 vs *Pv*1 and *Pf*10 vs *Pv*10, that are presented in Figs. 5–8, respectively. The characteristics of the spectra are discussed in the four spectral ranges, the 1200–1000 cm^{-1} and 3000–2850 cm^{-1} regions sensitive to the conformation of the hydrocarbon chains and the interchains interactions, respectively, the next region 1500–1200 cm^{-1} of the pyrrole ring stretching and CH_2/CH_3 deformation and the 1700–1500 cm^{-1} region of the core size marker bands.

3.4. PCA analysis of the Raman microspectroscopy data

3.4.1. C–C stretching vibration region (1200–1000 cm^{-1})

This spectral region includes the acyl backbone C–C bonds vibrations sensitive to the phospholipids molecular arrangement [32]. In this spectral range there are also bands characterizing heme vibrations [48, 49]. The PCA scores plots (Fig. 5A, 6A, 7A, 8A) show the separation based mainly on differences in the structurally sensitive bands found in this region.

*Pf*1 vs *Pf*10. The C-C stretching region shows a clear separation for the 1st and 10th day of *P. falciparum* infected patient data in the PC-1 vs PC-3 scores plot, Fig. 5A. The band at 1080 cm^{-1} observed on the 1st hospitalization day is due to the *ν*CC *gauche* conformer vibrations, while at 1068 cm^{-1} it is assigned to the *ν*CC *trans* conformation and typifies the process of returning to the health balance of the erythrocyte membrane. The 1102 cm^{-1}, PO_2^- symmetrical stretching of the phospholipids, observed for the 1st day is shifted to a lower frequency 1090 cm^{-1} on the 10th day. This describes that disorder still present in the membrane phospholipids assemblages [32]. Other minima bands in the PC-3 loadings, 1037 cm^{-1} (Ser), 1138 cm^{-1} (Asp), 1152 cm^{-1} (Thr), are assigned to amino acid residues associated with the invasion of the parasite and with the foreign proteins introduced into the membrane (Table 1).

*Pv*1 vs *Pv*10. The PC-1 vs PC-2 scores plot shows the separation of *Pv*1 and *Pv*10 data (Fig. 6 A). The similar minima positions in the PC-2 loadings plot, slightly shifted in relation to the correlation for *P. falciparum*, describe the *Pv*1 group (Table 1). It can be seen, however, that the data characterizing Pf10, due to some ambiguity, do not give a picture of a fully healthy membrane.

Summing up these two cases the Raman spectra from the first days of hospitalization for both *Plasmodia*, *Pf*1 and *Pv*1, are characterized by a higher presence of *gauche* conformers, while the last examined day, the *Pf*10 and the *Pv*10, contain more *trans* conformers.

*Pf*1 vs *Pv*1. The obtained PCA resulting in the PC-3 vs PC-4 scores plot, shows a distinction between the two groups of *Plasmodia* infected RBCs, *P. falciparum* and *P. vivax*, at the beginning of hospitalization (Fig. 7 A). The maxima in the PC-3 position loadings in the first days indicate wavenumbers of 1032 cm^{-1} (Ser), 1130 cm^{-1} (CC *trans*, PE), to *P. vivax*, while minima 1147 cm^{-1} (Asp, Glu), 1189 cm^{-1} (Tyr, Ser) and also 1170 cm^{-1} (Tyr, Ser) distinguishes *P. falciparum*. This dependence draws attention the signals from the amino acids influencing the recognition of the Raman spectra of blood cells changed under the influence of *P. falciparum* and *P. vivax* at the beginning of the infection.

*Pf*10 vs *Pv*10. The last day of hospitalization shows a clear separation of the data of both types of *Plasmodium* infected RBCs according to the PC-2 main component with a relatively high 26% variation (Fig. 8 A). The *P. falciparum* effect is characterized by the bands 1025 cm^{-1} (Ser), 1066 cm^{-1} (Arg) and 1090 cm^{-1} (*ν*CC *gauche*), while the *P. vivax* is

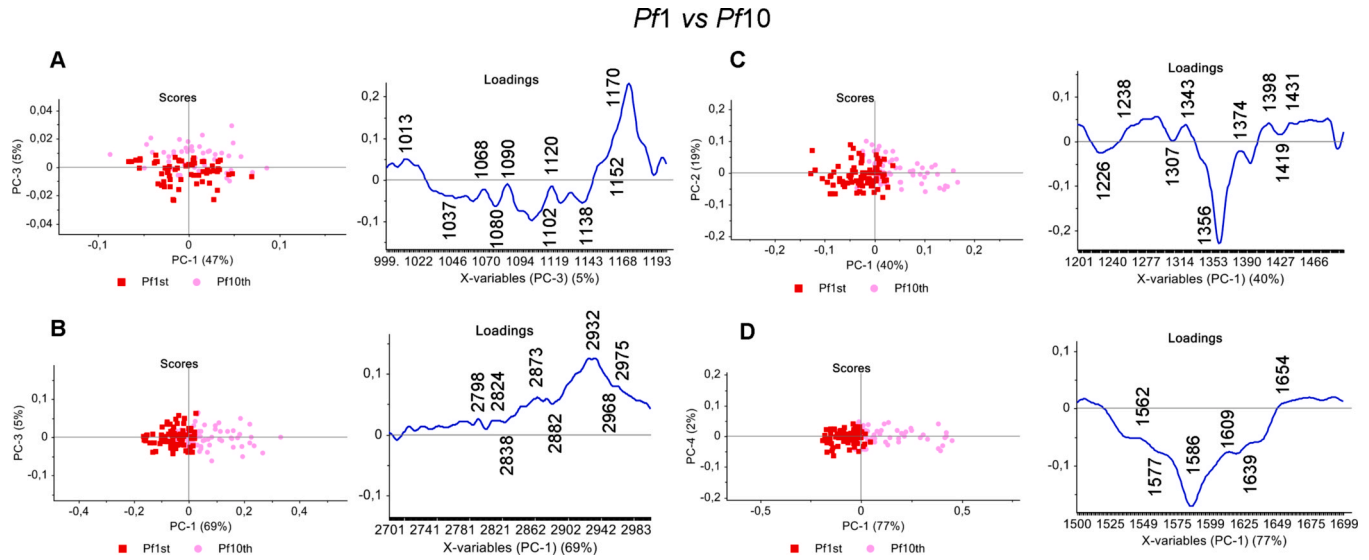

Fig. 5. Principal Component Analysis applied to Raman spectra of single RBCs, showing a general separation between patients infected with *P. falciparum* malaria parasites on the 1st day of hospitalization (red dots) and 10th day of hospitalization (pink dots); (A) PC-1 vs PC-3 scores plot and PC-3 loading plot, 1200–1000 cm^{-1} range; (B) PC-1 vs PC-3 scores plot and PC-1 loading plot, 3000–2700 cm^{-1} range; (C) PC-1 vs PC-3 scores plot and PC-3 loading plot, 1500–1200 cm^{-1} range; (D) PC-1 vs PC-2 scores plot and PC-2 loading plot, 1700–1500 cm^{-1} range; excitation laser line at 514.5 nm.

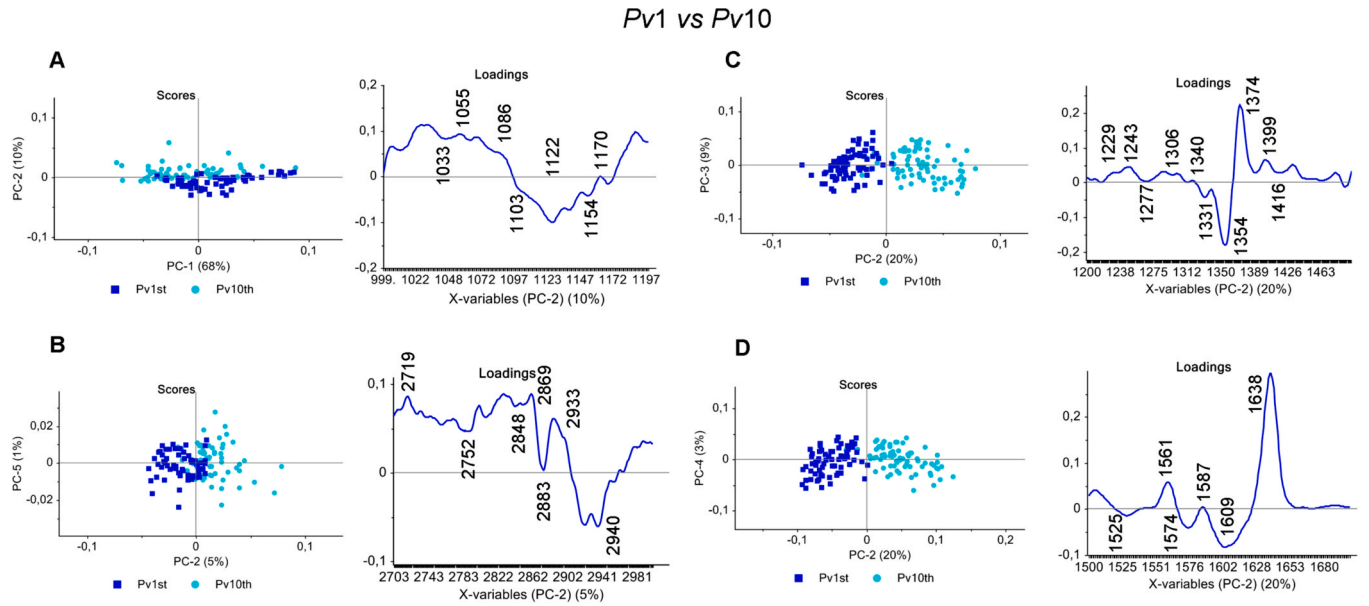

Fig. 6. Principal Component Analysis applied to Raman spectra of single RBCs, showing a general separation between patients infected with *P. vivax* malaria parasites on the 1st day of hospitalization (blue dots) and 10th day of hospitalization (turquoise dots); (A) PC-1 vs PC-3 scores plot and PC-3 loading plot, 1200–1000 cm^{-1} range; (B) PC-1 vs PC-4 scores plot and PC-4 loading plot, 3000–2700 cm^{-1} range; (C) PC-1 vs PC-3 scores plot and PC-3 loading plot, 1500–1200 cm^{-1} range; (D) PC-2 vs PC-3 scores plot and PC-2 loading plot, 1700–1500 cm^{-1} range; excitation laser line at 514.5 nm.

characterized by the bands 1124 cm^{-1} (ν_{22}) and 1170 cm^{-1} (Ser, Tyr).

3.4.2. *The C–H stretching vibration region (3000–2850 cm^{-1})*

In the area of the C-H stretching vibrations, inter-chain vibrations occur, which supplement information about the intra-chain C-C vibrations occurring in the area discussed earlier, enriching the obtained structural information concerning the membrane of the infected erythrocytes [32]. Bands at 2933 $cm^{-1}$and 2872 cm^{-1} are assigned to the symmetric and antisymmetric C–H stretching vibrations of the methyl and methylene groups, which originate from the saturated lipids in the malaria infected cells, Table 2 [55,56].

*Pf*1 vs *Pf*10 and *Pv*1 vs *Pv*10. The band of about 2930 cm^{-1} in the PC-1 and PC-2 loadings for *Pf*1 vs *Pf*10 and *Pv*1 vs *Pv*10, respectively, indicate the still existing disorder in the membrane caused by *Plasmodium* activity as well as the mixing of *Plasmodial* membranes (Fig. 5B, and 6B) [32,56]. Therefore, the amplification of the 2930 cm^{-1} band reflect the change in the environment of the CH_3 groups in proteins towards the more polar [57]. This indicates the normalization of the erythrocyte membrane and the return to the state typical for healthy erythrocytes which is expected on the 10th day of hospitalization.

*Pf*1 vs *Pv*1. The positive loadings on PC-2 indicate on the 2830 cm^{-1} and 2890 cm^{-1} bands due to overtone vibration, Glu and also PC asymmetric CH_2 vibrations, that specify *Pf*1. The opposite, negative PC-2 loadings, bands at 2721 cm^{-1}, 2761 cm^{-1}, which are overtones of

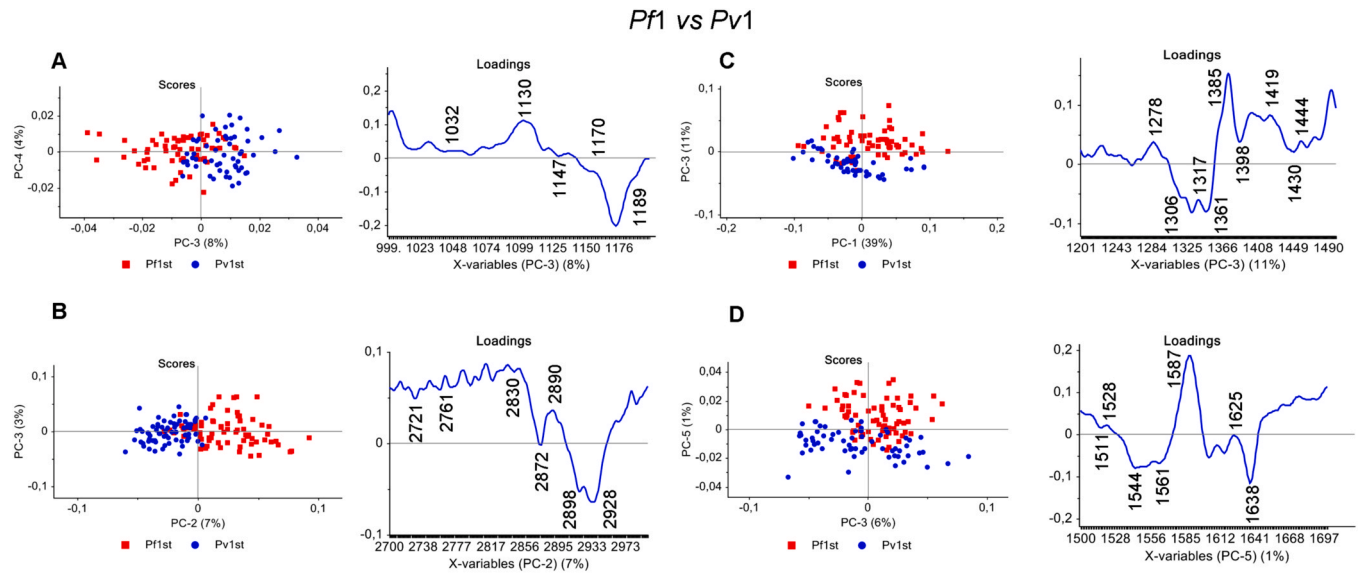

Fig. 7. Principal Component Analysis applied to Raman spectra of single RBCs, showing a general separation between patients infected with malaria parasites on the 1st day of hospitalization, *P. falciparum* (red dots) and *P. vivax* (blue dots); (A) PC-1 vs PC-2 scores plot and PC-2 loading plot, 1200–1000 cm^{-1} range; (B) PC-1 vs PC-3 scores plot and PC-3 loading plot, 3000–2700 cm^{-1} range; (C) PC-1 vs PC-2 scores plot and PC-2 loading plot, 1500–1200 cm^{-1} range; (D) PC-1 vs PC-4 scores plot and PC-4 loading plot, 1700–1500 cm^{-1} range; excitation laser line at 514.5 nm.

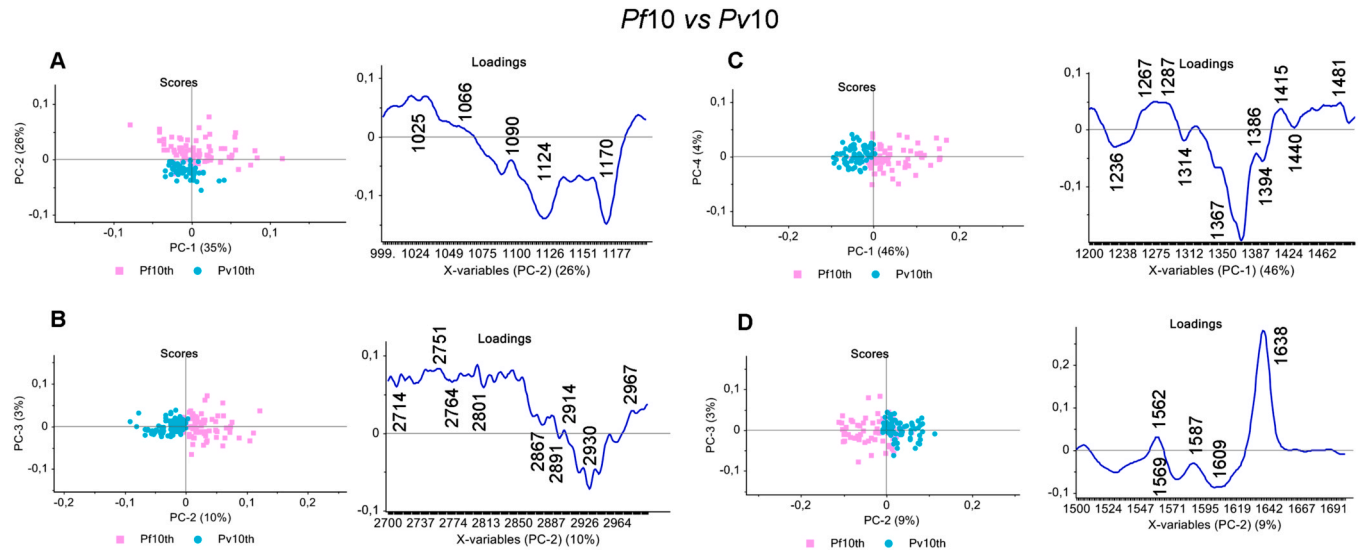

Fig. 8. Principal Component Analysis applied to Raman spectra of single RBCs, showing a general separation between patients infected with malaria parasites on the 10st day of hospitalization, *P. falciparum* (pink dots) and *P. vivax* (turquoise dots); (A) PC-1 vs PC-2 scores plot and PC-2 loading plot, 1200–1000 cm^{-1} range; (B) PC-2 vs PC-3 scores plot and PC-3 loading plot, 3000–2700 cm^{-1} range; (C) PC-1 vs PC-2 scores plot and PC-1 loading plot, 1500–1200 cm^{-1} range; (D) PC-1 vs PC-2 scores plot and PC-1 loading plot, 1700–1500 cm^{-1} range; excitation laser line at 514.5 nm.

heme and Asp vibrations, respectively, and 2872 cm^{-1}, 2898 cm^{-1} and 2928 cm^{-1} assigned to the methylene asymmetric stretching vibrations are characterized *Pv*1 (Fig. 7B). The methylene asymmetric stretching vibrations primarily indicate changes, disorder, that have occurred in the lipid bilayer of the erythrocyte, which seem to be dominated in the *P. vivax* infection. The presence of the Raman shifts of the selected amino acids, Glu and Asp, indicates the importance of the transport and metabolism of the carbohydrates found in red blood cells [58].

*Pf*10 vs *Pv*10. The C-H stretch area shows a separation in the PC-2 vs PC-3 scores plot for the last measurement day, comparing the cases of infection by each of the parasite species. The *Pv*10 is marked by the negative loadings on the PC-3 plot, by 2714 cm^{-1} (2 × ν_4; deoxyHb), 2764 cm^{-1} (2 ×ν_4; oxyHb), 2891 cm^{-1} (PC-outer), 2930 cm^{-1}, while *Pf*10 is signified by positive loadings, 2751 cm^{-1} (2 × $\nu(CH_2)$, PC-outer), 2801 cm^{-1}, 2914 cm^{-1} (2 ×δCH_2, DLPE-inner), 2967 cm^{-1} (ν_{asym} CH_3) (Fig. 8B). There are many characteristic bands of phospholipids, derived from the components of the inner- and outer- layer, and many of them are caused by *P. falciparum*. This is consistent with the data that the total lipid content of the infected RBCs is much higher than that of the healthy ones [56]. Therefore, this increased lipid content is probably due to the *Plasmodial* membrane phospholipids.

3.4.3. *Pyrrole ring stretching and the CH_2/CH_3 deformation region (1500–1200 cm^{-1})*

In this spectral range, in the PC-1 vs PC-2 scores plots, many changes related to the phenomenon of resonance Raman enhancement of pyrrole ring vibrations can be noticed. A principal component of PC-1 and PC-2 explains as much as 40% and 20% of the variability in the data in this

Table 1
The observed Raman bands positions and their assignment for single RBCs: for the patients infected with *P. falciparum* and *P. vivax* malaria parasites on the 1st and the 10th day of hospitalization: *Pf*1 vs *Pf*10, *Pv*1 vs *Pv*10, *Pf*1 vs *Pv*1 and *Pf*10 vs *Pv*10; 1200–1000 cm^{-1} range, 514.5 nm laser line.

Patients				Assignments[4,5,28–31,33,34,36,41,42,51,59]
*Pf*1	*Pf*10	*Pv*1	*Pv*10	
Raman band positions [cm^{-1}]				
*Pf*1 vs *Pf*10				
	1013			Phe
1037				νC-O, Ser
	1068			ν_{sym} C-C (*trans*), Arg
1080				ν_{sym} C-C (*gauche*); PE, inner layer
	1090			$\nu_{23,}$ $\nu(C_\beta\text{-}C_1)_{asym}$, (oxyHb); ν_{sym} C-C (*gauche*); ν(O-P-O$^-$); SM-inner layer
1102				ν_{sym} PO_2^-
	1120			$\nu_{22,}$ ν(pyr half-ring)$_{asym}$, (deoxyHb)
1138				νC-O, Asp, Glu
1152				νC-O, Thr
	1170			δC-OH, Tyr; γ(CH_2), Ser
*Pv*1 vs *Pv*10				
		1033		νC-O, Ser
			1055	ν_{sym} C-C (*trans*)
			1086	$\nu_{23,}$ $\nu(C_\beta\text{-}C_1)$ $_{asym}$; ν_{sym} C-C (*gauche*);
		1103		ν_{sym} PO_2^-
		1122		$\nu_{22,}$ ν(pyr half-ring)$_{asym}$, (deoxyHb); νC-C, PE-inner
		1154		νC-O, Thr
			1170	$\nu_{30,}$ ν(pyr half-ring)$_{asym}$; δC-OH, Tyr; γ(CH_2), Ser
*Pf*1 vs *Pv*1				
1032				νC-O, Ser
		1130		νC-C (*trans*); PE- inner layer
1147				νC-O, Asp, Glu
		1170		$\nu_{30,}$ ν(pyr half-ring)$_{asym}$; δC-OH, Tyr; γ(CH_2), Ser
1179				δC-OH, Tyr; γ(CH_2), Ser
*Pf*10 vs *Pv*10				
	1025			νC-O, Ser
	1066			ν_{sym} C-C (*trans*); Arg
	1090			$\nu_{23,}$ $\nu(C_\beta\text{-}C_1)_{asym}$, (oxyHb); ν_{sym} C-C (*gauche*);
			1124	$\nu_{22,}$ ν(pyr half-ring)$_{asym}$, (deoxyHb); νC-C, PE-inner
			1170	$\nu_{30,}$ ν(pyr half-ring)$_{asym}$; δC-OH, Tyr; γ(CH_2), Ser

Table 2
The observed Raman bands positions and their assignment for single RBCs: for the patients infected with *P. falciparum* and *P. vivax* malaria parasites on the 1st and the 10th day of hospitalization: *Pf*1 vs *Pf*10, *Pv*1 vs *Pv*10, *Pf*1 vs *Pv*1 and *Pf*10 vs *Pv*10; 3000–2700 cm^{-1} range, 514.5 nm laser line.

Patients				Assignments[5,27–30,32–34,51,59]
*Pf*1	*Pf*10	*Pv*1	*Pv*10	
Raman band positions [cm^{-1}]				
*Pf*1 vs *Pf*10				
	2798			$2 \times \nu_{20,}$ ν(pyr quater-ring) (oxyHb)
	2824			2 × ν(CN), Glu; 2 × ν(CC), Trp
2833				2 × ν(CN), Glu
	2873			ν_{asym} (CH_2)
2882				ν_{asym} (CH_2)
	2932			ν_{asym} (CH_3); $\nu_{11} + \nu_{41}$
2968				ν_{asym} (CH_3) in-plane
	2975			ν_{asym} (CH_3) in-plane
*Pv*1 vs *Pv*10				
			2719	$2 \times \nu_4$ (deoxyHb)
		2752		$2 \times \omega(CH_2)$, PC-outer
		2848		ν_{sym} (CH_2) (lipids); PC, SM –outer layer
			2869	ν_{asym} (CH_2)
		2883		ν_{asym} (CH_2); DLPE- inner layer
			2933	ν_{asym} (CH_3); $\nu_{11} + \nu_{41}$
			2940	ν_{sym} (CH_2) (lipids); PE-inner
*Pf*1 vs *Pv*1				
		2721		$2 \times \nu_4$ (deoxyHb)
		2761		$2 \times \nu_4$ (oxyHb); $2 \times \delta(CH_3)$, Asp
2830				2 × ν(CN), Glu
		2872		ν_{asym} (CH_2)
2890				ν_{asym} (CH_2), PC-outer; ν_{sym} (CH_2 + CH_3)
		2898		ν_{sym} (CH_2), ν_{sym} (NH_3^+), PE-inner
		2928		ν_{asym} (CH_3), PC-outer; ν_{11} + ν_{41}
*Pf*10 vs *Pv*10				
			2714	$2 \times \nu_4$ (deoxyHb)
	2751			$2 \times \omega(CH_2)$, PC-outer layer
			2764	$2 \times \nu_4$ (oxyHb)
	2801			$2 \times \nu_{20,}$ ν(pyr quater-ring) (oxyHb)
			2867	ν_{asym} (CH_2)
			2891	ν_{asym} (CH_2), PC-outer layer
	2914			$2 \times \delta(CH_2)$, DLPE-inner layer
			2930	ν_{asym} (CH_3); PC-outer; ν_{11} + ν_{41}
	2967			ν_{asym} (CH_3) in-plane

spectral range for *Pf*1 vs *Pf*10 and *Pv*1 vs *Pv*10, respectively, Table 3.

*Pf*1 vs *Pf*10. The negative PC-1 loadings, that depict the 1st hospitalization day, is marked by 1226 cm^{-1} (PE –inner layer; His), 1307 cm^{-1}, 1356 cm^{-1} (ν_4, significant deoxy Hb marker band) and 1419 cm^{-1} bands (Glu) (Fig. 5C). The strong positive PC-1 loading is primarily a 1374 cm^{-1} band, the Raman ν_4, oxy Hb and hemozoin (Hz) biomarker. The other bands are the 1238 cm^{-1} (ν_{42}; Hz), 1307 cm^{-1} (ν_{21}; Hz), 1343 cm^{-1}, 1398 cm^{-1} (ν_{20}; Hz), and 1431 cm^{-1} (Fig. 5C). The formation of Hz characterizes red blood cells already in the 1st but also in the 10th day of hospitalization (Table 3).

*Pv*1 vs *Pv*10. The PC-2 loading negative loading, describing the 1st day of hospitalization, is distinct by a band of 1354 cm^{-1} (ν_4, considerable deoxyHb marker band) in addition to the bands of amino acids side chains, such as Trp or Arg, while the last day of hospitalization is evident by a negative loading band of 1374 cm^{-1} (ν_4). Other bands that define the 10th day of hospitalization are also 1243 cm^{-1} (ν_{13}), 1306 cm^{-1} (ν_{21}), all due to oxy Hb, 1399 cm^{-1} (ν_{20}), originated from Hz and Glu (Fig. 6C). Here again, oxy Hb structure and hemozoin formation characterizes the red blood cells on the 10th day of hospitalization.

*Pf*1 vs *Pv*1. The PC-3 principal component on the PC-1 vs PC-3 scores plot separates data with 11% data variability. The positive PC-3 loadings plot indicates the amide III α-helical arrangement for *Pf*1 and also other characteristic vibrations of the pyrrole ring. But there are also deformation vibrations of phosphatidylcholine (PC), the phospholipid component of the outer layer of the erythrocyte membrane (Fig. 7 C). The negative PC-2 loadings plot indicates other lines typical of heme aggregation, Hz formation, for *Pv*1. The negative 1361 cm^{-1} band is usually correlated with the indole side chain environment and indicates buried Trp residue [32]. This band may point to the presence of tryptophan rich antigens (TRAg) [39].

*Pf*10 vs *Pv*10. The PC-1 vs PC-4 scores plot distinguishes patients data from the last day of hospitalization infected with *P. falciparum* and *P. vivax*. The bands for certain amino acids, such as Gln and Arg, appear actually for both species, but with slightly different band energies. An important band is represented by the signal of 1367 cm^{-1} from Trp, depicting the *Pv* infected RBCs on a 10th day of hospitalization. This band position indicates a different local environment of Trp residue than that on the first day of hospitalization. The variability of the PC-1 principal component, which separates groups, is rather high, 46%

Table 3
The observed Raman bands positions and their assignment for single RBCs: for the patients infected with *P. falciparum* and *P. vivax* malaria parasites on the 1st and the 10th day of hospitalization: *Pf*1 vs *Pf*10, *Pv*1 vs *Pv*10, *Pf*1 vs *Pv*1 and *Pf*10 vs *Pv*10; 1500–1200 cm^{-1} range, 514.5 nm laser line.

Patients				Assignments[5,28,29,31,33,34,42,48,51,59]
*Pf*1	*Pf*10	*Pv*1	*Pv*10	
Raman band positions [cm^{-1}]				
*Pf*1 vs *Pf*10				
1226				$\nu_{asym}PO_2^-$, PE –inner layer; His
	1238			$\nu_{42,}$ $\delta(C_mH)$, Hz; ν(CO), ν(CC), Tyr
1307				saturated fatty acids in lipids
	1343			$\nu_{41,}$ ν(pyr half-ring)$_{sym}$; δ(CH), endoplasmic reticulum; Glu
1356				$\nu_{4,}$ ν(pyr half-ring)$_{sym}$,(deoxyHb)
	1374			$\nu_{4,}$ ν(pyr half-ring)$_{sym}$ (oxyHb); Hz; PC-outer layer
	1398			$\nu_{20,}$ ν(pyr quater-ring); Hz; Asp
1419				$\delta(CH_2)$, DLPE–inner layer; Glu
	1431			$\nu_{28,}$ $\nu(C_\alpha C_m)$ $_{sym}$;
*Pv*1 vs *Pv*10				
			1229	ν_{13} or $\nu_{42,}$ $\delta(C_mH)$ (oxy Hb); $\nu_{asym}PO_2^-$, PE –inner layer
			1243	$\nu_{13,}$ (oxy Hb)
		1277		δ(CH), ν(CN), Trp
			1306	$\nu_{21,}$ $\delta(C_mH)$ (oxy Hb);
		1331		$\delta(CH_3)$, Trp; Arg
			1340	$\nu_{41,}$ ν(pyr half-ring)$_{sym}$; δ(CH), endoplasmic reticulum; Glu
		1354		$\nu_{4,}$ ν(pyr half-ring)$_{sym}$ (deoxyHb)
			1374	$\nu_{4,}$ ν(pyr half-ring)$_{sym}$ (oxyHb)
			1399	$\nu_{20,}$ ν(pyr quater-ring); Hz; Asp
		1416		$\delta(CH_2)$, DLPE-inner layer
*Pf*1 vs *Pv*1				
1278				amide III (α-helix); ν(CN), Trp
		1306		$\nu_{21,}$ $\delta(C_mH)$, Hz;
1317				$\nu_{23} + \nu_{26}$ $\nu(C_\alpha C_\beta)$+ $\delta(C_\alpha C_m)$; Glu
		1361		$\delta_s(CH_3)$, Trp
1385				$\delta_s(CH_3)$, Asp
		1398		$\nu_{20,}$ ν(pyr quater-ring); Hz; Glu
1419				$\nu_{28,}$ $\nu(C_\alpha C_m)$ $_{sym}$ (deoxyHb);
		1430		$\nu_{28,}$ $\nu(C_\alpha C_m)$ $_{sym}$ (deoxyHb); Trp
1444				$\delta(CH_2)$, PC-outer layer
*Pf*10 vs *Pv*10				
			1236	$\nu_{42,}$ $\delta(C_mH)$, Hz; ν(CO), ν(CC), Tyr
	1267			amide III (α-helix), ν(CO), ν(CC), Tyr; δ(=CH) in-plane, unsaturated fatty acids in lipids
	1287			δ(COH), Asp, Gln
			1314	δ(CH), Trp
			1367	$\nu_{4,}$ ν(pyr half-ring)$_{sym}$ (oxyHb); Asp
	1386			$\nu_{4,}$ ν(pyr half-ring)$_{sym}$ (oxyHb); δ (CH_3), Asp
			1394	$\nu_{20,}$ ν(pyr quater-ring);
	1415			ν(CN), Gln
			1440	$\gamma(CH_2)$, PE, SM; His
	1481			$\delta(CH_3)$, Phe

(Fig. 8C). The signal from unsaturated fatty acids in the lipids for *Pf*10 is noteworthy.

3.4.4. Core size marker band region (1700–1500 cm^{-1})

Pf1 vs *Pf10*. This spectral range shows the separation in the PC-1 vs PC-4 scores plot, for the analyzed model of RBCs infected with *P. falciparum*, and is described by a variability of PC-1 equal to 77%. The positive shifts in the PC-1 loadings plot, showing the characteristics on 10th day of treatment, marks the band 1562 cm^{-1} (ν_2) resulting from Hz, and 1639 cm^{-1} (ν_{10}, and Arg). The first day of hospitalization is featured by 1586 cm^{-1} (ν_{38}, Hz and Glu), 1577 cm^{-1} (Asp), 1609 cm^{-1} (ν_{19}), Fig. 5D.

Pv1 vs *Pv10*. We have observed a variability of the marker bands in the PC-2 vs PC-4 scores plot (Fig. 6D). The first day of hospitalization is characterized by 1525 cm^{-1} (ν_2 and Lys), 1574 cm^{-1} (Asp), 1609 cm^{-1} (ν_{19}), in the positive PC-2 loadings plot. The last day of hospitalization is distinguished by marker bands, 1561 cm^{-1} from ν_2, 1587 cm^{-1} from ν_{37}, and 1638 cm^{-1} associated with Gln and ν_{10}.

Pf1 vs *Pv1*. The positive PC-5 loadings are indicative for the first day of *P. falciparum,* and is differentiated by vibrations at: 1528 cm^{-1} originated from ν_{28} of Hz and also Lys, 1587 cm^{-1} originated from ν_{32} of Hz and Gln and 1625 cm^{-1} due to amino acids, Lys and Tyr. The positive PC-4 loadings plots describes the first day of hospitalization with *P. vivax* infection, and shows the 1511 cm^{-1} bands from Trp, then 1544 cm^{-1}, 1561 cm^{-1} and 1638 cm^{-1} from ν_{13}, ν_2 and ν_{10}, respectively (Fig. 7D). The PC-5 principal component separates the two modeled groups *Pf*1 and *Pv*1 which is mainly due to the different structure of the heme, which, is Hz aggregates already formed or the oxy-Hb structure, respectively.

Pf10 vs *Pv10*. The PC-2 vs PC-3 scores plot shows a 9% variance, due to PC-2, that models data specifying the 10th day of hospitalization for infection with *P. falciparum* and *P. vivax*. The PC-2 principal component differentiates the ν_2 and ν_{19} vibrations indicating oxy-Hb for *P. falciparum* infection in relation to *P. vivax* vibrations 1562 cm^{-1} of Glu, 1587 cm^{-1} coming from ν_2 and Gln and 1638 cm^{-1} due to ν_{10} and Arg (Fig. 8D). For the infected *P. falciparum* cells, structural changes in the heme become typical, while for the infected *P. vivax* cells also significant are vibrations indicating Hz and amino acids such as Glu, Gln and Arg. The relevant data, band positions and assignments are provided in Table 4.

4. Summary and Conclusions

For the first time to our knowledge the differences in red blood cells caused by protozoa, *P. falciparum* and *P. vivax*, the most common *Plasmodia species* causing malaria, were discriminated using Raman spectroscopy.

The corresponding to *P. falciparum* spectroscopic data are more scattered than that of *P. vivax*, and this characteristic applies to all of the

Table 4
The observed Raman bands positions and their assignment for single RBCs: for the patients infected with *P. falciparum* and *P. vivax* malaria parasites on the 1st and the 10th day of hospitalization: *Pf*1 vs *Pf*10, *Pv*1 vs *Pv*10, *Pf*1 vs *Pv*1 and *Pf*10 vs *Pv*10; 1700–1500 cm^{-1} range, 514.5 nm laser line.

Patients				Assignments[5,28,29,31,33,34,42,48,51]
*Pf*1	*Pf*10	*Pv*1	*Pv*10	
Raman band positions [cm^{-1}]				
*Pf*1 vs *Pf*10				
	1562			$\nu_{2,}$ $\nu(C_\beta C_\beta)_{asym}$, (oxyHb)
1577				$\nu(COO^-)$, Asp
1586				$\nu_{37,}$ $\nu(C_\alpha C_m)_{asym}$, Hz; $\delta(NH_2)$, Glu
1609				$\nu_{19,}$ $\nu(C_\alpha C_m)_{asym}$
	1639			$\nu_{10,}$ $\nu(C_\alpha C_m)_{asym}$ (oxyHb); Arg
	1654			amide I (α)
*Pv*1 vs *Pv*10				
		1525		$\nu_{sym}(NH_3^+)$, Lys
			1561	$\nu_{2,}$ $\nu(C_\beta C_\beta)_{asym}$, (oxyHb)
		1574		$\nu_{2,}$ $\nu(C_\beta C_\beta)_{asym}$, Hz; ν_{asym} (COO^-), Asp
			1587	$\nu_{37,}$ $\nu(C_\alpha C_m)_{asym}$, Hz; $\delta(NH_2)$, Gln
		1609		$\nu_{19,}$ $\nu(C_\alpha C_m)_{asym}$
			1638	amide I (α) ; $\nu_{10,}$ $\nu(C_\alpha C_m)_{asym}$ (oxyHb); Arg
*Pf*1 vs *Pv*1				
		1511		ν(CN), Trp
1528				$\nu_{38,}$ ν (pyr breathing); Hz; $\nu_{sym}(NH_3^+)$, Lys
		1544		$\nu_{13,}$ ν (pyr breathing); Trp
		1561		$\nu_{2,}$ $\nu(C_\beta C_\beta)_{asym}$, (oxyHb)
1587				$\nu_{37,}$ $\nu(C_\alpha C_m)_{asym}$, Hz; $\delta(NH_2)$, Gln
1625				ν_{10}; Hz; ν(C = C), Tyr, Lys
		1638		amide I (α); $\nu_{10,}$ $\nu(C_\alpha C_m)_{asym}$ (oxyHb); Arg
*Pf*10 vs *Pv*10				
			1562	$\nu_{2,}$ $\nu(C_\beta C_\beta)_{asym}$, ν_{asym} (COO^-), Glu
	1569			$\nu_{2,}$ $\nu(C_\beta C_\beta)_{asym}$, (oxyHb)
			1587	$\nu_{37,}$ $\nu(C_\alpha C_m)_{asym}$, Hz; $\delta(NH_2)$, Glu
	1609			$\nu_{19,}$ $\nu(C_\alpha C_m)_{asym}$
			1638	amide I (α) ; $\nu_{10,}$ $\nu(C_\alpha C_m)_{asym}$ (oxyHb); Arg

spectral ranges in the measurements (Figs. 5–8). This observation seems to be connected with other specificity of changes in erythrocytes possibly due to parasite considerable heterogeneity.

The differences observed in this spectral range on the first day of hospitalization for *P. falciparum* versus *P. vivax* in the 1200–1000 cm^{-1} range fluctuate by 8% due to the second component of PC-3. More significant, the difference observed on the tenth day of hospitalization differs significantly in the second PC-2 loadings plot with the high percentage of variation, equal to 26%. This spectral range describes the acyl backbone vibrations. It consists of many C-C bonds, and thus allow to determine the intra-chain phospholipids organization. There are noticeable changes in membrane proteins amino acids content. For *P. falciparum* there is Asp, Glu, Ser content enhancement. While for *P. vivax* there is Tyr content increase as well as changes in the cytoplasm membrane inner layer. On the tenth day of hospitalization, when the healing process is advanced, the greatest difference in the effects caused by both species of the parasitic protozoa is observed, which is probably related to the tropism of *P. vivax* towards reticulocytes. It is necessary to point out the observed ambiguities in assignments in the scope characterizing structural changes in the membrane may be caused by a significant amount of *Plasmodium* lipids and proteins in the composition of the membrane.

The pyrrole ring stretching region, 1500–1200 cm^{-1}, contains some discriminating changes. When comparing the spectra from the first and tenth day of hospitalization, considering these spectroscopic data as a comparison of respectively infected and healthy RBCs, the variability in the heme structure is dominant, which is indicated primarily by the ν_4 oxidation state marker band (see Fig. 4). In addition to the heme marker vibrations, there are also vibrations characteristic of Hemozoin (Hz), aggregated forms of heme, and Raman bands associated with the protein side chains, e.g. Trp, Tyr, Arg and Asp, see Table 3. The differences between the results induced by the two species of parasites appearing on the first day of hospitalization indicate the alterations in heme vibrations as characteristic of *P. falciparum*, while the presence of aggregated forms of heme, and Hz as well as Trp and Glu side chains for *P. vivax*. The strong negative loadings at c.a. 1360 cm^{-1} is indicative for the *P. vivax* infected RBCs on the first day of hospitalization pointing to the Trp band, Fig. 7C. The 1361 cm^{-1} band, of Trp increases if the environment is hydrophobic, which is in this case. The presence of the Trp signal seems to indicate the process of ligand-receptor complex formation as a result of *P. vivax* invasion. The invasion of *P. falciparum* occurs with the basigin receptor which requires glycosylation involved with the aspartic acid groups. The positive PC-3 loading at 1385 cm^{-1} is attributed to the Asp vibrations and may mark a formation a receptor–ligand connection. The tenth day of hospitalization was ascertained by Asp 1386 cm^{-1} and Trp 1367 cm^{-1} vibrations for *P. falciparum* and *P. vivax*, respectively, Table 3. The vibration observed for *P. vivax* for the Trp indole ring significantly shifted towards higher wavenumbers which may indicate a very strong hydrophobic interaction.

Core size marker band region, 1700–1500 cm^{-1} considering that at the beginning of hospitalization patients infected with *Plasmodium* the strong positive PC-5 loadings at 1587 cm^{-1} can be observed for the *P. falciparum* which may be attributed to the Gln vibrations, Fig. 7D. It seems to indicate the formation of a ligand-receptor complex by *P. falciparum* Erythrocyte Membrane Protein 1 (PfEMP1). Whereas at the beginning of hospitalisation patients with *P. vivax* the shift observed at 1544 cm^{-1} PC-5 negative loadings is due to Trp an indole ring vibration, and it seems to be consistent with the previously discussed 1361 cm^{-1} vibration, which indicates the invasion stage of the parasite, the formation of the ligand-receptor complex - Transferrin receptor (TfR). The tenth day of hospitalization is distinguished with a 9%, variance of PC-2 due to vibrations typical for heme (in the *P. falciparum* case) and to heme, and also amino acids: Glu, Gln and Arg, (in *P. vivax* case). Raman spectroscopy distinguishes ligand-receptor interactions between different species of the parasite and human host erythrocytes, although they exhibit considerable heterogeneity and molecular evolution, which can lead to the observed data dispersion. Despite all the limitations in obtaining a simple answer, which was to distinguish the effect of the specious of *Plasmodium* on blood cells, it seems we have been able to observe the trend of change characteristic of each type of *Plasmodium*.

Due to the intention of our work to contribute to the advancement of translational medicine, Raman research do not require much effort in routine hospital work, as the blood smear didn't need any staining or complicated preparation, and at the moment some insight into the specifics of malaria infection. This gives a likely possibility to use of Raman spectroscopy in clinical practise in future.

Declaration of Competing Interest

The authors declare that they have no known competing financial interests or personal relationships that could have appeared to influence the work reported in this paper.

Acknowledgements

The study was funded by the research part of the subsidy of the Faculty of Chemistry of the Jagiellonian University in Krakow, Poland. MB-Z acknowledges the support of InterDokMed project no. POWR.03.02.00-00-I013/16, Poland.

Appendix A. Supporting information

Supplementary data associated with this article can be found in the online version at doi:10.1016/j.clispe.2021.100015.

References

[1] World malaria report 2019, World Health Organization (2019) Printed in France, ISBN 978–92-4–156572-1.
[2] T.H. Dzbeński, Epidemiological situation of malaria in Poland - past, present and future. Wiad. Parazytol, 54 (2008) 205–211.
[3] Infectious diseases and poisonings in Poland in 2017, Chief Sanitary Inspectorate – Department for Communicable Disease and Infection Prevention and Control, Warszawa 2019.
[4] M. Kozicki, J. Czepiel, G. Biesiada, P. Nowak, A. Garlicki, A. Wesełucha-Birczyńska, The ring-stage of Plasmodium falciparum observed in RBCs of hospitalized malaria patients, Analyst 140 (2015) 8007–8016, https://doi.org/10.1039/c5an01598g.
[5] A.G. Maier, K. Matuschewski, M. Zhang, M. Rug, Plasmodium falciparum, Trends Parasitol. 35 (2019) 481–482, doi.org/10.1016/j.pt.2018.11.010.
[6] G.E. Weiss, B.S. Crabb, P.R. Gilson, Overlaying molecular and temporal aspects of malaria parasite invasion, Trends Parasitol. 32 (2016) 284–295, doi.org/10.1016/j.pt.2015.12.007.
[7] I. Mueller, M.R. Galinski, J.K. Baird, J.M. Carlton, D.K. Kochar, P.L. Alonso, H. A. del Tortillo, Key gaps in the knowledge of Plasmodium vivax, a neglected human malaria parasite, Lancet Infect. Dis. 9 (2009) 555–566, https://doi.org/10.1016/S1473-3099(09)70177-X.
[8] J.K. Baird, Evidence and implications of mortality associated with acute Plasmodium vivax malaria, Clin. Microbiol. Rev. 26 (2013) 36–57, https://doi.org/10.1128/CMR.00074-12.
[9] N.M. Douglas, G.J. Pontororing, D.A. Lampah, T.W. Yeo, E. Kenangalem, J. R. Poespoprodjo, A.P. Ralph, M.J. Bangs, P. Sugiarto, N.M. Anstey, R.N. Price, Mortality attributable to Plasmodium vivax malaria: a clinical audit from Papua, Indonesia, BMC Med. 12 (217) (2014) 1–13, doi.org/10.1186/s12916-014-0217-z.
[10] P.W. Gething, I.R.F. Elyazar, C.L. Moyes, D.L. Smith, K.E. Battle, C.A. Guerra, A. P. Patil, A.J. Tatem, R.E. Howes, M.F. Myers, D.B. George, P. Horby, H.F. L. Wertheim, R.N. Price, I. Mueller, J.K. Baird, S.I. Hay, A long neglected world malaria map: Plasmodium vivax endemicity in 2010, PLoS Negl. Trop. Dis. 6 (1–12) (2012), 1814, https://doi.org/10.1371/journal.pntd.0001814.
[11] Diagnostic testing for malaria, World Health Organization, ⟨https://www.who.int/activities/diagnostic-testing-for-malaria⟩ (Accessed 10.03.2021).
[12] Malaria Diagnosis (U.S.) – Microscopy, Diagnostic Tools, Centers for Disease Control and Prevention, ⟨https://www.cdc.gov/malaria/diagnosis_treatment/diagnostic_tools.html#⟩ (Accessed 10.03.2021).
[13] A.F. Cowman, J. Healer, D. Marapana, K. Marsh, Malaria: BIOLOGY AND DISEAse, Cell 167 (2016) 610–624, doi.org/10.1016/j.cell.2016.07.055.
[14] J. Czepiel, S. Goldman, A. Szlauer-Stefańska, A. Mielimonka, G. Biesiada, A. Kalinowska-Nowak, A. Wesełucha-Birczyńska, W. Perucki, A. Garlicki, Delay in diagnosis and treatment of patients with cases of imported malaria in Poland – one center's experience, Fam. Med. Prim. Care Rev. 19 (2017) 93–97, doi.org/10.5114/fmpcr.2017.67859.
[15] Guidelines for the Treatment of Malaria. Treatment of Plasmodium vivax, P. ovale, P. malariae and P. knowlesi infections, third ed., World Health Organization, 2015, pp. 285–299.

[16] Treatment of Malaria: Guidelines for Clinicians (United States), Centers for Disease Control and Prevention, ⟨https://www.cdc.gov/malaria/diagnosis_treatment/clinicians1.html#⟩ (access 10.03.2021).

[17] A. Khoshmanesh, M.W.A. Dixon, S. Kenny, L. Tilley, D. McNaughton, B.R. Wood, Detection and quantification of early-stage malaria parasites in laboratory infected erythrocytes by attenuated total reflectance infrared spectroscopy and multivariate analysis, Anal. Chem. 86 (2014) 4379–4386, doi.org/10.1021/ac500199x.

[18] M.R. Galinski, J.W. Barnwell, Plasmodium vivax: who cares, Malar. J. 7 (1) (2008) 9, https://doi.org/10.1186/1475-2875-7-S1-S9.

[19] M.R. Galinski, J. Barnwell. Nonhuman Primate Models for Human Malaria Research, Nonhuman Primates in Biomedical Research: Diseases, second ed., Academic Press Elsevier, 2012, pp. 299–323, https://doi.org/10.1016/B978-0-12-381366-4.00005-5.

[20] J.M. Carlton, A.A. Escalante, D. Neafsey, S.K. Volkman, Comparative evolutionary genomics of human malaria parasites, Trends Parasitol. 24 (12) (2008) 545–550, https://doi.org/10.1016/j.pt.2008.09.003.

[21] A.F. Cowman, C.J. Tonkin, W.-H. Tham, M.T. Duraisingh, The molecular basis of erythrocyte invasion by malaria parasites, Cell Host Microbe 22 (2017) 232–245, dx.doi.org/10.1016/j.chom.2017.07.003.

[22] M.R. Galinski, E.V.S. Meyer, J.W. Barnwell, Plasmodium vivax: modern strategies to study a persistent parasite's life cycle, Adv. Parasitol 81 (2013) 1–26, doi.org/10.1016/B978-0-12-407826-0.00001-1.

[23] F.B. Cogswell, The hypnozoite and relapse in primate malaria, Clin. Microbiol. Rev. 5 (1) (1992) 26–35, https://doi.org/10.1128/cmr.5.1.26.

[24] M.R. Galinski, M. Xu, J.W. Barnwell, Plasmodium vivax reticulocyte binding protein-2 (PvRBP-2) shares structural features with PvRBP-1 and the Plasmodium yoelii 235 kDa rhoptry protein family, Mol. Biochem. Parasitol. Rev. 108 (2) (2000) 257–262, 10.1016/s0166-6851(00)00219-x.

[25] T. Bousema, C. Drakeley, Epidemiology and infectivity of Plasmodium falciparum and Plasmodium vivax gametocytes in relation to malaria control and elimination, Clin. Microbiol. Rev. 24 (2) (2011) 377–410, 10.1128/CMR.00051-10.

[26] S.E. Francis, D.J. Sullivan Jr., D.E. Goldberg, Hemoglobin Metabolism in the Malaria Parasite Plasmodium Falciparum, Annu. Rev. Microbiol. 51 (1997) 97–123, https://doi.org/10.1146/annurev.micro.51.1.97.

[27] J.M. Pisciotta, D. Sullivan, Hemozoin: oil versus water, Parasitol. Int. 57 (2008) 89–96, https://doi.org/10.1016/j.parint.2007.09.009.

[28] D.E. Goldberg, A.F.G. Slater, The pathway of hemoglobin degradation in malaria parasites, Parasitol. Today 8 (1992) 280–283, doi.org/10.1016/0169-4758(92)90146-S.

[29] M. Birczyńska-Zych, J. Czepiel, M. Łabanowska, M. Kurdziel, G. Biesiada, M. Kozicki, A. Garlicki, A. Weselucha-Birczynska, The aging of P. falciparum infected RBCs by 2D-correlation Raman and EPR Spectroscopy, J. Mol. Struct. 1224 (1–12) (2021), 129036 doi.org/10.1016/j.molstruc.2020.129036.

[30] S.C. Goheen, L.J. Lis, O. Kucuk, M.P. Westerman, J.W. Kauffman, Compositional dependence of spectral features in the Raman spectra of erythrocyte membranes, J. Raman Spectrosc. 24 (1993) 275–279, https://doi.org/10.1002/jrs.1250240503.

[31] A. Wesełucha-Birczyńska, M. Kozicki, J. Czepiel, M. Łabanowska, P. Nowak, G. Kowalczyk, M. Kurdziel, M. Birczyńska, G. Biesiada, T. Mach, A. Garlicki, Human erythrocytes analyzed by generalized 2D Raman correlation spectroscopy, J. Mol. Struct. 1069 (2014) 305–312, https://doi.org/10.1016/j.molstruc.2014.03.023.

[32] A.T. Tu, Raman Spectroscopy in Biology: Principles and Applications, John Wiley & Sons, New York, 1982.

[33] E. Lenzi, S. Dinarelli, G. Longo, M. Girasole, V. Mussi, Multivariate analysis of mean Raman spectra of erythrocytes for a fast analysis of the biochemical signature of ageing, Talanta 221 (1–8) (2021), 121442, https://doi.org/10.1016/j.talanta.2020.121442.

[34] A.F. Cowman, B.S. Crabb, Invasion of red blood cells by malaria parasites, Cell 124 (2006) 755–766, https://doi.org/10.1016/j.cell.2006.02.006.

[35] M. Zhang, P. Faou, A.G. Maier, M. Rug, Plasmodium falciparum exported protein PFE60 influences Maurer's clefts architecture and virulence complex composition, Int. J. Parasitol. 48 (2018) 83–95, doi.org/10.1016/j.ijpara.2017.09.003.

[36] C. Crosnier, L.Y. Bustamante, S.J. Bartholdson, A.K. Bei, M. Theron, M. Uchikawa, S. Mboup, O. Ndir, D.P. Kwiatkowski, M.T. Duraisingh, J.C. Rayner, G.J. Wright, Basigin is a receptor essential for erythrocyte invasion by Plasmodium falciparum, Nature 480 (2011) 534–537, https://doi.org/10.1038/nature10606.

[37] D.C. Stein, V. Briken, Microbial glycobiology!Antigenic variation of microbial surface glycosylated molecules, Struct. Relev. Appl. (2010) 819–835, https://doi.org/10.1016/B978-0-12-374546-0.00041-9.

[38] J. Gruszczyk, R.K. Huang, L.-J. Chan, S. Menant, C. Hong, J.M. Murphy, Y.-F. Mok, M.D.W. Griffin, R.D. Pearson, W. Wong, A.F. Cowman, Z. Yu, W.-H. Tham, Cryo-EM structure of an essential Plasmodium vivax invasion complex, Nature 559 (2018) 135–139, doi.org/10.1038/s41586-018-0249-1.

[39] U. Kanjee, G.W. Rangel, M.A. Clark, M.T. Duraisingh, Molecular and cellular interactions defining the tropism of Plasmodium vivax for reticulocytes, Curr. Opin. Microbiol. 46 (2018) 109–115, doi.org/10.1016/j.mib.2018.10.002.

[40] H. Takeuchi, Raman structural markers of tryptophan and histidine side chains in proteins, Biopolymers 72 (2003) 305–317.

[41] U. Kanjee, G.W. Rangel, M.A. Clark, M.T. Duraisingh, Molecular and cellular interactions defining the tropism of Plasmodium vivax for reticulocytes, Curr. Opin. Microbiol. 46 (2018) 109–115, doi.org/10.1016/j.mib.2018.10.002.

[42] J.M. Pisciotta, P.F. Scholl, J.L. Shuman, V. Shualev, D.J. Sullivan, Quantitative characterization of hemozoin in Plasmodium berghei and vivax, Int. J. Parasitol. Drugs Drug Resist. 7 (2017) 110–119, doi.org/10.1016/j.ijpddr.2017.02.001.

[43] G. Fontecha, A. Pinto, D. Escobar, G. Matamoros, B. Ortiz, Genetic variability of Plasmodium falciparum histidine-rich proteins 2 and 3 in Central America, Malaria J. 18 (2–10) (2019) 31, https://doi.org/10.1186/s12936-019-2668-3.

[44] M.C. Leclerc, P. Durand, C. Gauthier, S. Patot, N. Billotte, M. Menegon, C. Severini, F.J. Ayala, F. Renaud, Meager genetic variability of the human malaria agent Plasmodium vivax, PNAS 101 (2004) 14455–14460, https://doi.org/10.1073/pnas.0405186101.

[45] B.M. Cooke, N. Mohandas, R.L. Coppel, The malaria-infected red blood cell: structural and functional changes, Adv. Parasitol. 50 (2001) 1–86, 0065-308X.

[46] J. Czepiel, M. Kozicki, P. Panasiuk, M. Birczyńska, A. Garlicki, A. Wesełucha-Birczyńska, Clostridium difficile the hospital plague, Analyst 140 (2015) 2513–2522, https://doi.org/10.1039/c4an01947d.

[47] C. Lavazec, Molecular mechanisms of deformability of Plasmodium-infected erythrocytes, Curr. Opin. Microbiol. 40 (2017) 138–144, doi.org/10.1016/j.mib.2017.11.011.

[48] T. Kitagawa, Y. Ozaki, Infrared and Raman Spectra of Metalloporphyrins, Structure and Bonding, 64, Springer-Verlag, Berlin Heidelberg, 1987, pp. 72–114.

[49] B.R. Wood, D. McNaughton, Raman excitation wavelength investigation of single red blood cells in vivo, J. Raman Spectrosc. 33 (2002) 517–523, 10.1002/ jrs.870.

[50] D. McNaughton, B.R. Wood, Resonance Raman spectroscopy in malaria research, Expert Rev. Proteomics 3 (2006) 525–544, https://doi.org/10.1586/14789450.3.5.525.

[51] M. Abe, T. Kitagawa, Y. Kyogoku, Resonance Raman spectra of octaethylporphyrinato Ni(II) and meso-deuterated and 15N substituted derivatives. II. A normal coordinate analysis, J. Chem. Phys. 69 (1978) 4526–4534, https://doi.org/10.1063/1.436450.

[52] B.R. Wood, B. Tait, D. McNaughton, Micro-Raman characterisation of the R to T state transition of haemoglobin within a single living erythrocyte, BBA 1539 (2001) 58–70, doi.org/10.1016/S0167-4889(01)00089-1.

[53] B.R. Wood, K. Kochan, K.M. Marzec, Resonance Raman Spectroscopy of Hemoglobin in Red Blood Cells, Ch. 13, in Vibrational Spectroscopy in Protein Research, Elsevier, 2020 doi.org/10.1016/B978-0-12-818610-7.00013-X.

[54] B.R. Wood, S.J. Langford, B.M. Cooke, J. Lim, F.K. Glenister, M. Duriska, J. K. Unthank, D. McNaughton, Resonance Raman spectroscopy reveals new insight into the electronic structure of β-hematin and malaria pigment, J. Am. Chem. Soc. 126 (2004) 9233–9239, doi.org/10.1021/ja038691x.

[55] M. Kozicki, D.J. Creek, A. Sexton, B.J. Morahan, A. Wesełucha-Birczyńska, B. R. Wood, An attenuated total reflection (ATR) and Raman spectroscopic investigation into the effects of chloroquine on Plasmodium falciparum- infected red blood cells, Analyst 140 (2015) 2236–2246, https://doi.org/10.1039/c4an01904k.

[56] I.W. Sherman, Biochemistry of Plasmodium (Malarial Parasites), Microbiol. Rev. 43 (1979) 453–495, 01460749/79/04-0453/43.

[57] R.B. Mikkelsen, S.P. Verma, D.F.H. Wallach, Effect of transmembrane ion gradients on Raman spectra of sealed, hemoglobin-free erythrocyte membrane vesicles, Proc. Natl. Acad. Sci. U.S.A. 75 (1978) 5478–5482, https://doi.org/10.1073/pnas.75.11.5478.

[58] S.A. Desai, Why do malaria parasites increase host erythrocyte permeability? Trends Parasitol. 30 (2014) 151–159, https://doi.org/10.1016/j.pt.2014.01.003.

[59] J. De Gelder, K. De Gussem, P. Vandenabeele, L. Moens, Reference database of Raman spectra of biological molecules, J. Raman Spectrosc. 38 (2007) 1133–1147, 10.1002/jrs.1734.